Dynamic ultimate strength of a ultra-large container ship subjected to realistic loading scenarios

George Jagite, Fabien Bigot, Sime Malenica, Quentin Derbanne, Herve Le Sourne, Patrice Cartraud

Dynamic ultimate strength of a ultra-large container ship subjected to realistic loading scenarios

George Jagite [a,*], Fabien Bigot [b], Sime Malenica [b], Quentin Derbanne [b], Herve Le Sourne [c], Patrice Cartraud [c]

[a] *Bureau Veritas, Research Department, Saint-Herblain 44807, France*
[b] *Bureau Veritas, Research Department, Paris 92937, France*
[c] *Ecole Centrale Nantes, GeM Institute UMR 6183 CNRS, Nantes 44321, France*

When technically specifying ships for the future, the following aspects are examples of what we will have even more focus on than today: bigger, lighter, and faster. Thereby, the hydroelastic type of structural response will be more and more significant. Furthermore, it is well-known that the whipping-induced stresses are having a higher frequency than the ordinary wave-induced stresses; hence, some doubts are cast on the probability that the dynamic effects may provide additional strength reserves. Therefore, this research aims to analyze the dynamic ultimate capacity of ultra-large container ships under realistic loading scenarios. The hull-girder is subjected to a combined bending moment, resulting from a long-term hydroelastic analysis, with the lateral loads and to local loads given by different cargo loading cases. The numerical results are discussed, and the dynamic load factors are derived as the ratio between the dynamic capacity and the quasi-static one. Finally, it is shown that the strain rate effect is negligible in the analysis of the ultimate strength of ship structures subjected to whipping-induced stresses.

1. Introduction

The future is all about water. The energy transition towards renewable energies, the need for extra land for the highly developed countries, and the increasing international transport by ships are a few of the challenges that engineers and researchers have to cope with. In consequence, more and more innovative structural solutions are needed. Notwithstanding that the modern world is driven by the need for environmentally friendly and economical designs, the following two aspects are of paramount importance for the designing of modern structures: (i) the accurate prediction of the environmental loads acting on the structures; (ii) the guarantee that the global structural strength is capable of withstanding an extreme loading scenario.

In general terms, the design condition for the ultimate strength of a structure can be expressed as follows:

$$\frac{\mathbf{M}_U}{\gamma_U} - \sum \gamma_L \mathbf{L}_i > 0 \tag{1}$$

where $\mathbf{M}_U$ is the ultimate strength and $\mathbf{L}_i$ is the ith load component; γ_U and γ_L are the characteristic safety factors associated with the ultimate strength and the load components, respectively. These safety factors are introduced in order to consider some uncertainties for the material properties, geometry, and scantlings, encountered loads, etc.

* Corresponding author.
E-mail address: george.jagite@bureauveritas.com (G. Jagite).

Regarding the ultimate strength of a ship's hull girder, the first evaluation has been made by means of analytical methods and can be attributable to [1]. In his work, he presumed a bending stress distribution over the hull cross-section, in which all structural components in compression are reaching their buckling plastic collapse state, and all components in tension are reaching a fully plastic state. Because the stress distribution presumed by Caldwell [1] was not representative for modern ship structures, several improved methods have been reported over the years [2,3]. These methods are assuming different stress distribution at collapse, taking into account plasticity and buckling. Although analytical methods are simple and easy to apply, these methods are not providing any information about the severity of the collapse.

Several years after [1] developed the first methodology of evaluating the ultimate strength, a new method was proposed by Smith [4], known as the progressive collapse method. In this method, the cross-section is divided into small elements composed of stiffeners and their attached plating. Each component has a specific load-shortening curve. Therefore, by increasing the curvature of a cross-section progressively and integrating the stresses from each component, results in a nonlinear moment–curvature diagram, where its peak value defines the structural capacity. In spite of their limitations related to the inability to handle initial imperfections or lateral loads, the methods based on the progressive collapse [4–7] are still in wide use because of the computational efficiency. During the last years, some more advanced progressive collapse methods have been proposed. Tanaka et al. [8] extended the Smith method to include the shear stresses in order to compute the ultimate strength of a ship section subjected to combined vertical bending and torsional moments. In their methodology, a correction of the average stress-average strain relationship is made to consider the effect of shear stress. Fujikubo and Tatsumi [9] proposed an extended method to account for the bottom lateral loads' effect. The double bottom is idealized as a grillage of beam elements, which allows the out-of-plane deflection due to the lateral loads.

A different numerical approach has been proposed by Ueda and Sherif [10], and it is known as the Idealized Structural Unit Method (ISUM). The structural units used in ISUM are more sophisticated than the elements used in the FEM (Finite Element Method) and are based on mathematical approximations [11,12]. However, the structural units are considerably bigger than the finite elements used in FEM. Hence, the computational time is significantly reduced. Several improvements to the ISUM have been reported over the years. Paik et al. [13] developed a program for the ultimate strength analysis of large structures composed of stiffened panels, using five types of ISUM units (beam–column unit, plate unit, stiffened plate unit, hard unit, and virtual unit). A summary of different ISUM theories and analysis of different possible applications of ISUM is presented in [14]. Fujikubo et al. [15] improved the existent ISUM formulation in order to include the effect of web buckling in bending. Underwood et al. [16] proposed a new ISUM for the ultimate strength analysis of damaged structures. Lindemann [17] improved the shape function for lateral pressure loads. Kaeding et al. [18] used the ISUM to analyze the collapse behavior of a VLFS. Paik et al. [19] validated the ultimate strength computed by ALPS/HULL software, based on ISUM, with the ultimate strength computed by NL-FEM analysis, using ANSYS software. Lindemann and Kaeding [20] used the ISUM for the analysis of the ultimate strength of stiffened plate structures under lateral pressure and in-plane stresses.

In the last decade, the rapid increase in computer performance led to the possibility of applying the nonlinear finite element method (NL-FEM) to perform complex collapse analysis of entire ship structures. Amlashi and Moan [21] analyzed the alternate hold loading effect on the ultimate strength of a bulk carrier. The FE results were used to contribute to the development of simplified methods for the analysis of ship hulls under combined global and local loads. Also, they documented some essential aspects of the methodology for the nonlinear FE modeling and analysis. Shu and Moan [22] studied the ultimate strength of a bulk carrier under an alternate hold loading condition using a three-cargo holds model. They found that the influence of different loading paths is relatively small. Moreover, it was found that the alternate hold loading condition decreases the ultimate strength by almost 37%. Pei et al. [23] used a complex ship model to analyze the collapse behavior of a bulk carrier under alternate hold loading conditions, finding that the structural capacity reduced by about 20%. Moreover, the double bottom bending of bulk carriers and oil tankers is covered within the Common Structural Rules for Bulk Carriers and Oil Tankers [24] by applying a partial safety factor. The applicability of this factor was discussed by Darie et al. [25]. Pei et al. [26] used a combined FEM/ISUM complete ship model of a bulk carrier to analyze the reduction of ultimate strength due to lateral pressure loads. The numerical results showed that the ultimate strength for hogging bending moments is reduced by 20%.

The ultimate strength of container ships under combined bending moment and lateral pressure loads has been investigated by Fujikubo and Tatsumi [9,27],Tatsumi and Fujikubo [28], showing that the lateral loads are reducing the ultimate strength by 18%. Mohammed et al. [29] analyzed the ultimate strength of container carriers under combined torsional and bending moments. It was shown that under a torsional moment approximately equal to the ultimate torsional moment, the ultimate strength under bending loads is reduced by less than 20%. This aspect was also investigated by Tanaka et al. [30]. Matsumoto et al. [31] investigated the effect of lateral loads on the hull girder ultimate strength of large container ships considering full load condition with an empty bay and without ballast in the double bottom. The analyses were conducted on eighteen container ships with various sizes between 4000 TEU and over 10000 TEU. The numerical results indicated that the lateral load effect would reduce the ultimate strength by up to 30%, depending on the ship configuration; for twelve of the considered ships, the ultimate strength reduction was around 10%. Tatsumi and Fujikubo [32] analyzed the effect of the combined hogging moment and bottom local loads over the ultimate strength of container ships. By performing progressive collapse analysis of two ULCS (Ultra-Large Container Ships), they concluded that the ultimate hogging strength is mainly reduced due to increased longitudinal thrust in the outer bottom plate and reduced effectiveness of the inner bottom plating.

In all the procedures mentioned above, the hull girder ultimate strength evaluation is performed under quasi-static conditions, disregarding the dynamic effects such as strain rate and inertia. However, the current practice for evaluating the hull girder ultimate strength of relatively 'soft' structures is to compare the maximum dynamic vertical bending moment after a slamming event, obtained from a hydroelastic analysis where the structural behavior is considered as linear and elastic, with the quasi-static

hull girder capacity which considers the nonlinear elastic–plastic structural behavior. Therefore, some doubts are cast on the current hydroelastic methods' capability to accurately predict the extreme dynamic response based on a linear elastic structural model. Aside from that, since the whipping-induced stresses have a higher frequency than the ordinary wave-induced stresses, the dynamic effects such as inertia and strain rate effects may provide additional strength reserves for the ship structure and should be investigated.

Going back to the literature, several researchers have analyzed the influence of the nonlinear structural behavior over the hydroelastic response through analytical methods, experimental tests, and numerical simulations, e.g., Iijima et al. [33],Xu et al. [34],Derbanne et al. [35],Iijima and Fujikubo [36]. However, to the authors' knowledge, there are no satisfactory studies, either numerical or experimental, on the hydroelastoplastic response of ships subjected to the slamming-induced whipping response. This aspect will be covered in a separate publication.

Regarding the influence of the dynamic effects on the ultimate strength, [37] has introduced a partial safety factor of 0.9, reducing the whipping effectiveness during the collapse. This coefficient represents the dynamic collapse effect. The primary assumption is that the strain rate and inertia effects may provide additional load carrying capacity when the hull girder structure is subjected to dynamic loads. Furthermore, several researchers focused on the dynamic effects of whipping-induced stresses on the ultimate strength of container ships. Yamada [38] investigated the effect of strain rate over the ultimate strength of a ULCS subjected to hogging bending moment, using a simple half-sine loading function. The numerical analyses found that the ultimate strength is increased by 10%–20% range due to the strain rate effect, depending on the loading period. However, this increased capacity observed by Yamada is due to the improper set of coefficients used in the Cowper–Symonds model and the methodology used to define the dynamic capacity. In a paper previously published by the authors Jagite et al. [39], we have investigated the dynamic ultimate strength of ULCS subjected to hogging bending moment. The FE models were extended over three frame bays and were subjected to pure bending moment using a simple half-sine loading function associated with typical periods for wave- and whipping-induced stresses. The dynamic ultimate strength was defined as the maximum load that the hull girder can withstand without collapsing, any load level higher than this level leading to structural failure. Finally, it was found that the dynamic capacity of the hull girder increased by less than 3% when the new definition of the dynamic ultimate strength was used.

The present research work continues the previous investigation reported by the authors [39], and the new objective is to analyze the influence of the dynamic effects over the hull girder ultimate strength under more realistic loading scenarios. The numerical investigations of the dynamic ultimate strength are performed using state-of-the-art nonlinear finite element analysis method where an ultra-large container ship with a cargo-carrying capacity of 16000 TEU is taken as a subject. The global external loads are determined from direct hydroelastic analysis by making use of an equivalent design wave (EDW) to maximize the vertical bending moment. The resulting time-series of bending moment are directly applied at both ends of the finite element model. At first, the dynamic ultimate strength is computed using a FE model extended over the three frame bays, and it is compared to the one obtained on simple half-sine loading scenarios. Secondly, a more complex FE model extended over two-hold is used to analyze a container ship's dynamic ultimate strength under complex loading scenarios. The loading scenarios considered are combining the global hull girder bending moment with the local loads due to different cargo scenarios and lateral pressures.

It is essential to mention that container ships are loaded over the full length most of the time. However, there exists a possibility of sailing with an empty hold. Such loading scenarios are mentioned in the classification societies rules, for example, [40], or in [41]. Thus, one of this paper's objectives is to investigate the ultimate strength of a container ship under an alternate loading condition. Therefore, two loading conditions are considered: full load condition with uniform cargo distribution, and full load condition with one-bay empty, without ballast in the double bottom.

The considered model has two watertight bulkheads (WBhd) that are delimiting a cargo hold. And each hold is divided into two 40-foot bays by a partial bulkhead (PBhd). A typical deformation of the double bottom under lateral loads is shown in Fig. 1. Moreover, in the scenario when the ship sails with one-bay empty and without ballast in the double bottom, the lateral loads' effect is significantly higher. Hence, the combined global and local bending might lead to a bigger reduction of the ultimate strength, as depicted in Fig. 1.

2. Theoretical background

2.1. Definition of the dynamic ultimate strength

At first, it is essential to differentiate the two main dynamic effects: inertia and strain rate. Firstly, the inertia of the structure affects the structural response, and mainly the amplitude of the internal load, which can be higher or lower than the applied external load. Secondly, the strain rate effect represents the dynamic enhancement of the yield strength and increases when the loading speed increases.

When analyzing the ultimate strength of a structure using a static simulation, the maximum load is clearly defined, since no static equilibrium can be found when this load level is exceeded. However, this is not true in the case of a dynamic simulation, where the load can theoretically be arbitrarily increased, the excess of load leading to an acceleration of the structure associated with very high distortion. Furthermore, when the dynamic effects are included in a dynamic simulation, it is necessary to use realistic load-amplitude curves. Moreover, it is critical how the dynamic collapse is defined. If the load applied during the dynamic analysis leads to collapse, then such a load level is of minimal interest for the designer. Therefore, when computing the dynamic ultimate strength, one should determine the maximum load that can be applied to the structure without collapsing; any load higher than this level will lead to structural collapse.

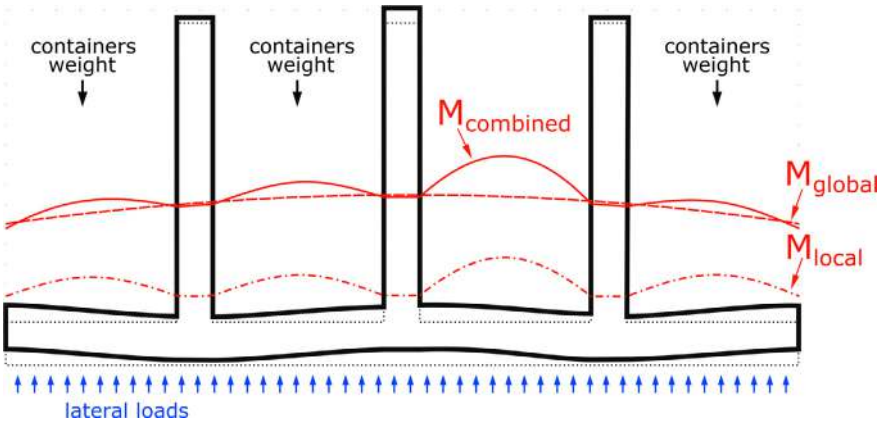

Fig. 1. Illustration of the global and local bending moments for one-bay empty condition.

In the current research work, the dynamic ultimate strength investigations are carried out numerically, using the state-of-the-art nonlinear finite element analysis software ABAQUS. Since it is necessary to perform the analyses in a time-domain solver, the Finite Element Analysis (FEA) solver of choice is the dynamic implicit solver, where both material and geometrical nonlinearities were taken into account.

Going back in the literature, it can be seen that in the studies reported by Jiang et al. [42], and Yamada [38] the load amplitude curves are fixed, where the maximum amplitude is set to 120% of the quasi-static structural capacity. It is worth mentioning that in both investigations, the Cowper–Symonds strain rate sensitivity model is used. Jiang et al. [42] defined the critical buckling load (i.e., the ultimate strength) as the applied load at the instant when the axial displacement accelerates rapidly. In the study by Yamada [38], the dynamic ultimate strength was defined as the maximum internal bending moment reached during the simulation. Moreover, in the studies by Jiang et al. [42], and Yamada [38] the structure largely collapses at the end of the simulation. This basically means that the load level reached during the collapse represents a load level that the structure cannot withstand. Aside from that, by applying a load level significantly higher than the quasi-static ultimate strength the strain rate effect will be overestimated.

In order to illustrate the limitations and errors induced by using an over-increased load approach, let us consider a partial hull girder structural model extended over three frame-bay in the longitudinal direction, subjected to pure bending. The ship's main particulars and the details of FE modeling can be found in Section 3.

At first, the quasi-static hull girder ultimate strength (i.e., without the dynamic effects) is computed using a static solver based on the arc-length method. For the analysis of the dynamic ultimate strength, the hull girder is subjected to a simple half-sine loading scenario. The loading period is 1.8 s, which may be considered a representative period of the slamming-induced whipping response. The amplitude of the external load M_{ext} is firstly set to 120% of the quasi-static structural capacity, denoted M_{U-QS}, as follows: $M_{ext} = 1.2 \cdot M_{U-QS}$. It should be mentioned that in a quasi-static simulation, the applied load M_{ext} is equal to the internal load M_{int}. However, this is no longer valid in dynamic computations when the external load differs from the internal one. The maximum internal bending moment reached during this dynamic scenario is $M_{int} = 1.145 \cdot M_{U-QS}$. Then, if a new scenario where the load amplitude is set to $M_{ext} = 1.145 \cdot M_{U-QS}$ is defined, the structure collapses again, and the maximum internal bending moment reached is $M_{int} = 1.126 \cdot M_{U-QS}$. Several such iterations are necessary until the load amplitude reaches a level that the structure can withstand. And thus, any higher load level will lead to structural collapse. For the considered partial structural model, the dynamic capacity is found when the applied load is $M_{ext} = 1.080 \cdot M_{U-QS}$. By increasing the load a little bit more, for a dynamic load $M_{ext} = 1.081 \cdot M_{U-QS}$, the structure collapses, as shown in Fig. 2.

In the methodology developed by the authors for the calculation of the dynamic capacity, it is considered that the structure collapsed when the structural deformation accelerates rapidly, with a rapid reduction in stiffness and the loss of structural stability. This can be seen in Fig. 2(c), showing the time variation of the end-rotation. Moreover, the structural collapse can also be determined from the variation of the internal loads: the structure collapses when the internal loads decrease sharply. Fig. 2(b) presents the time variation of the internal bending moment. Aside from that, the internal load vs. end-rotation curve is depicted in Fig. 2(d) from which we can infer that for a dynamic load, $M_{ext} = 1.080 \cdot M_{U-QS}$ the structure suffers permanent deformations without collapsing. By increasing the load a little bit more, for a dynamic load, $M_{ext} = 1.081 \cdot M_{U-QS}$, the end-displacement accelerates rapidly, and the structure collapses. Therefore, the maximum capacity of the stiffened panel is achieved for a dynamic load of $1.080 \cdot M_{U-QS}$.

In Fig. 3(a) it can be seen that the side girders, the bottom plating, and the attached stiffeners are showing concentrated plastic strains at the end of the unloading phase, but the structure has enough strength to withstand a load of $1.080 \cdot M_{U-QS}$. However, suppose the load is increased a little bit more. In that case, the structure collapses, the bottom plating and the attached stiffeners are losing their stability and develop significant out-of-plane deformations, as Fig. 3(b) bears out.

The numerical results depicted in Fig. 2, are showing the necessity of developing a new approach for determining the dynamic ultimate strength of a structure. The dynamic ultimate strength represents the maximum load that the structure can withstand without collapsing and should be calculated using an iterative approach. For practical reasons, it is more convenient to start from

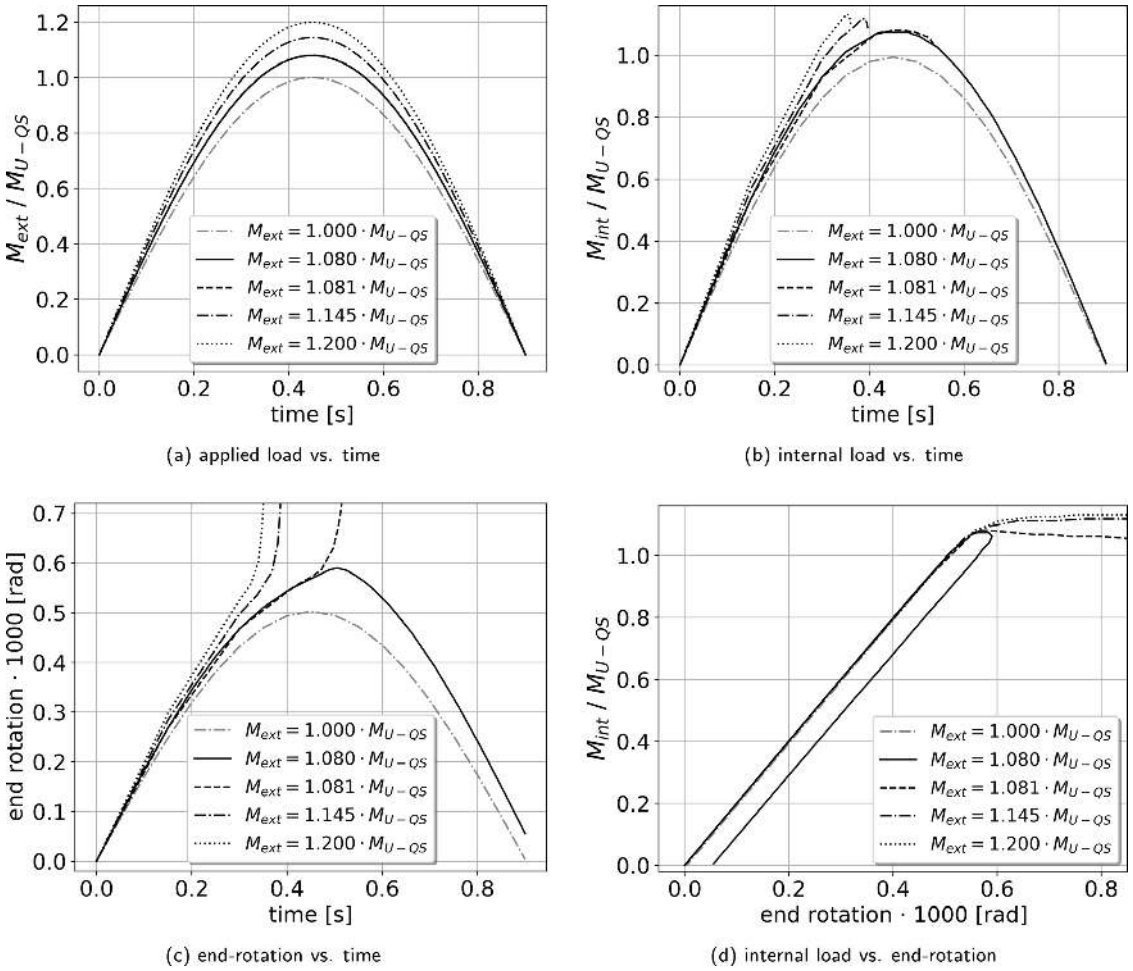

Fig. 2. Definition of dynamic structural collapse.

the quasi-static ultimate strength and to increase the load amplitude. It should be mentioned that each iteration requires a dynamic simulation to be solved in the time domain. Hence, the entire procedure can become extremely costly. With regard to this, an adaptive iteration step was chosen until the difference between a non-failure scenario and a failure scenario is less than $0.001 \cdot M_{U-QS}$.

2.2. Strain rate sensitivity

Dynamic load effects can induce changes in the material strength properties, and many researchers showed that the plastic flow of some materials is sensitive to strain rate. This may be regarded as a property of steel, and it is well-known that mild steel and titanium alloys exhibit this behavior most strongly, while high tensile steels, on the other hand, are much less strongly affected.

Early experiments reported by Manjoine [43] showed that the lower yield stress and the ultimate tensile stress increased with an increase in the strain rate for low-carbon steels. A few years later, [44] gathered all experimental results and proposed the constitutive Eq. (2) for the strain rate sensitive materials, which is used extensively in numerical studies.

$$\frac{\sigma_d}{\sigma_0} = 1 + \left(\frac{\dot{\varepsilon}}{C}\right)^{1/q} \tag{2}$$

where σ_0 represents the quasi-static yield stress, σ_d represents the dynamic yield stress obtained at strain rate $\dot{\varepsilon}$. C and q are the Cowper–Symonds parameters.

A similar investigation of the dynamic tensile behavior of low carbon mild steel specimens was reported by Campbell and Cooper [45] for a wide range of strain rates, between 10^{-5} and 10^{2} s^{-1}. The experimental results showed that the lower and upper yield stresses are increasing when the strain rate is increasing, similar to the results of Manjoine [43]. However, the ultimate tensile stress increases more slowly.

Within the investigations performed by the Ship Structural Committee, several reports have been published regarding the effect of strain rate on the toughness of ship steels [46,47].

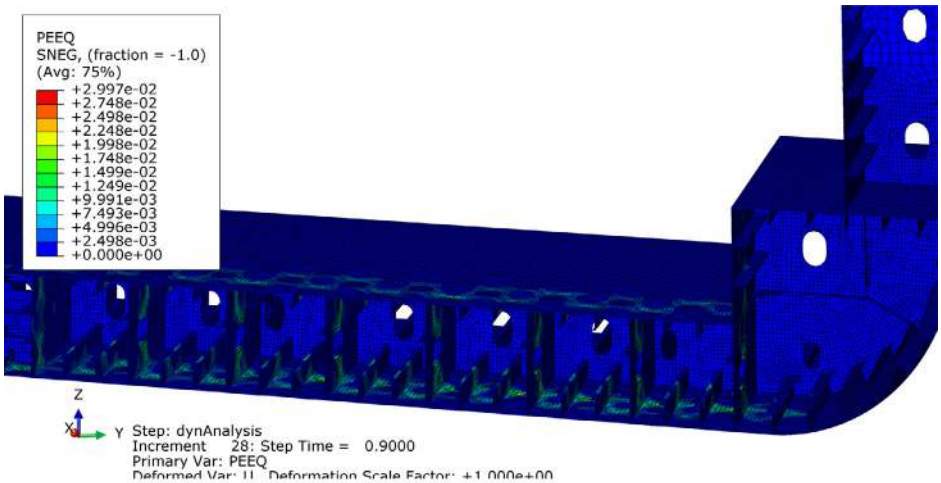

(a) non-failure scenario, $1.080 \cdot M_{U-QS}$ (after unloading the structure)

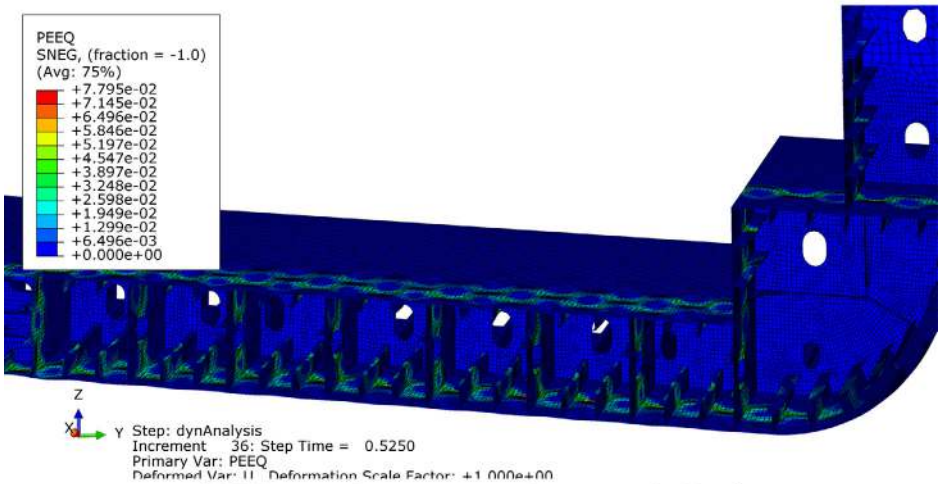

(b) failure scenario, $1.081 \cdot M_{U-QS}$ (at structural collapse)

Fig. 3. Equivalent plastic strains distribution. (deformation factor = 1.0)

Rolfe et al. [46] proposed preliminary criteria for ensuring adequate structural properties of a broad range of ship steels. The hypothesis proposed by Rolfe et al. [46] was further evaluated by Francis et al. [48] in SSC-275 by performing dynamic yield stress tests for seven grades of ship steels, including mild steel and high tensile steel. Laboratory experiments were performed at various strain rates and temperatures. For the static yield stress, a strain rate of $1.3 \cdot 10^{-4}$ s^{-1} was used, for the dynamic case, a strain rate of $8 \cdot 10^{-3}$ s^{-1}, and for the impact case, a strain rate of 5 s^{-1}. The experimental results show that the dynamic yield stress is equal to the static yield stress plus a dynamic over-stress, which is temperature-dependent. The results are in good agreement with the assumption introduced in SSC-244 [46].

However, some materials used for the previously reported experimental investigations are not relevant anymore since they are no longer in use. Therefore, in the last ten years, several researchers [49–51] reported on the strain rate sensitivity of various steels used in shipbuilding.

Choung et al. [50] proposed a new formula to estimate the material constant C of Cowper–Symonds constitutive equation, while the second constant is fixed, $q = 5$. Tensile tests were carried out at five strain rate levels from quasi-static to intermediate strain rates, and different temperature conditions, low temperature, room temperature, and high temperature.

$$C = \alpha + \beta\varepsilon_p^2 \tag{3}$$

Based on the experimental test results for *DH36* and *EH36* steels, [50] proposed Eq. (3), where coefficients α and β are listed in Table 1, and ε_p denotes the plastic strain.

Moreover, [50] compared the dynamic yield stress obtained using Eq. (3) with the results obtained using [52] equation, which is derived from dynamic tensile test data of automobile sheet plates. Lee and Kim [52] proposed Eq. (4) to approximate the material

Table 1
Cowper Symonds' constant C coefficients.

	α	β	Constant C		
			$\varepsilon_p = 0.05$	$\varepsilon_p = 0.10$	$\varepsilon_p = 0.15$
DH36	5.54e4	8.54e6	8.02e4	1.36e5	2.50e5
EH36	8.95e4	3.29e7	3.96e5	4.66e5	5.84e5

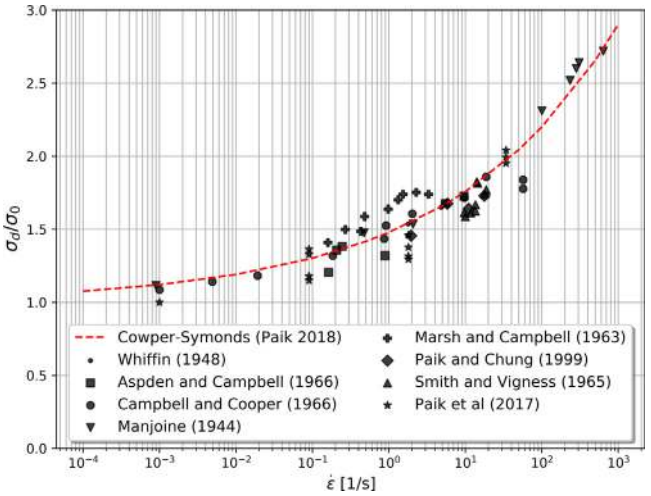

Fig. 4. Dynamic yield stress ratio of mild steel.

constant C, while the value of the second constant is fixed, $q = 5$.

$$C = \begin{cases} 92000 \cdot \exp\left(\dfrac{\sigma_0}{364}\right) - 19400 & \text{if } \sigma_0 > 270 \text{ MPa} \\ 40 & \text{if } \sigma_0 \leq 270 \text{ MPa} \end{cases} \tag{4}$$

Paik et al. [51] developed a new test database of the mechanical properties of materials for marine applications, including mild steel and high tensile steel. The test database covers strain rates between 10^{-3} and 10^{2} s^{-1} and temperatures between room temperature, low temperature, and cryogenic temperature. The new experimental results for the dynamic yield stress ratio of mild steels are in very good agreement with the Cowper–Symonds constitutive equation, as Fig. 4 bears out. It should be noted that in the tests of Paik et al. [51], the static yield stress was determined for a strain rate of 10^{-3} s^{-1}, which does not correspond with the recommendations of international standards. According to the classification societies rules [53,54], for the determination of the upper yield stress, R_{eH}, the test shall be carried out with an elastic stress rate between 6 and 60 MPa s^{-1}. On the other hand, in order to minimize the measurement uncertainty, ISO [55] proposed a different method to be used when the strain rate sensitive parameters are analyzed. For determination of the upper yield stress, R_{eH}, the strain rate shall be kept as constant as possible, between $7 \cdot 10^{-5}$ and $2.5 \cdot 10^{-4}$ s^{-1}.

For the high tensile steel, the comparison between experimental results and the Cowper–Symonds constitutive equation is presented in Fig. 5. The coefficients proposed by Paik [56] are giving a better approximation at low strain rates (i.e., less than 1 s^{-1}) if we consider the experimental test results obtained on modern materials used in marine constructions. Therefore, in order to analyze the strain rate effect on the dynamic ultimate strength, the following constants: $C = 3200$, $q = 5$ were used for the Cowper–Symonds constitutive material model, presented in Eq. (2).

As it can be seen in Fig. 5, the considered strain rate sensitivity model shows increased yield stress by around 5% at strain rates as low as 10^{-3} s^{-1}. This is in direct contradiction with the experimental results that assume the static yield stress for a strain rate of 10^{-3} s^{-1}. Moreover, since under wave-induced stress, the strain rates on the hull girder are around 10^{-3} s^{-1}, the existent Cowper–Symonds model contradicts the long-established industry practice to consider the wave loads as quasi-static and disregard the dynamic effects associated with the wave loads.

2.3. Hydroelastic model

The hydroelastic analyses are performed using the software HOMER, developed and maintained by Bureau Veritas. Within HOMER, the fully coupled hydroelastic problem is solved using the generalized modes approach, as described in [57]. The natural modes can be calculated either using a 1D beam model or the full 3D FEM model of the ship structure. After solving the general seakeeping problem in the frequency domain using a 3D Boundary Element Method (BEM) based on Green's sources, the time-domain

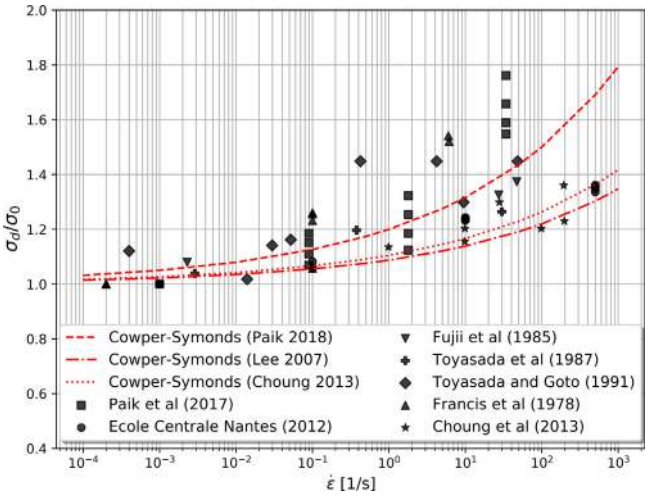

Fig. 5. Dynamic yield stress ratio of high tensile steel.

simulation is performed following the approach proposed by Cummins [58]. Aside from that, several nonlinear effects are added, such as the Froude–Krylov correction and the slamming loads, which are calculated using the Generalized Wagner Model [59]. The method allowed for the computation of springing and whipping responses and was validated with both experimental and full-scale results [60].

For the evaluation of the ultimate strength, the objective of the hydroelastic analysis is to predict extreme events. There are two principal design methodologies for identifying maximum hydrodynamic loads, including the nonlinear effects: equivalent design waves (EDW) and design sea-state [61]. Due to practical reasons, in this research work, the time series of the vertical bending moment are determined from an EDW using the North Atlantic scatter diagram [62]. Therefore, a response conditioned wave (RCW) is created to maximize the nonlinear vertical bending moment (VBM) response at midship. The RCW is defined as an irregular wave train containing several components leading to the mean of the possible responses on a uni-directional sea-state. More details about the advantages of using uni-directional response conditioned waves (RCW) can be found in [61,63–65].

It should be mentioned that by computing the loads using a hydroelastic model, and applying them on a nonlinear elasto-plastic structural model leads to some inconsistencies. This is due to the fact that the available hydroelastic models are computing the wave- and slamming-induced loads as the internal loads of a linear elastic structural model. However, in reality, the collapse of the hull girder is not resulting from the imposed forces, nor displacements (rotations). Instead it results from the interaction between the collapsing structure and the loads acting on the structure. Thus, there is a need for hydroelastoplastic models in order to consider the nonlinearties existing in both the structural and hydrodynamic problems.

Such a model has been recently developed by the authors and published in [66]. The fully-coupled hydroelastoplastic method is used to determine the influence of nonlinear structural behavior on the extreme wave- and slamming-induced loads on a board range of ships. The nonlinear whipping response, defined as the response of a nonlinear elastoplastic structural model, has been compared to the linear whipping response obtained using a linear-elastic structural model. It was found that the effect of the nonlinear structural behavior on whipping response varies from 0.1% to 2.4%, reducing the amplitude of the internal loads. This can be explained by the fact that a certain amount of the waves' energy is dissipated in the form of plastic deformation in the hull girder. Finally, it is concluded that the nonlinear structural behavior can be neglected in the analysis of the maximum hydroelastic response. Therefore, within the current research work, it is assumed that the influence of the nonlinear structural response in the analysis of the extreme hydrodynamic loads is negligible.

3. Numerical data

3.1. Ship particulars

An ultra-large container ship with a cargo-carrying capacity of 16000 TEU is taken as a subject. The midship section is shown in Fig. 6(a), and the geometry of the model is shown in Fig. 6(c). In the previous investigation reported by the authors [39], a numerical model extended over three frame-bay has been used, as shown in Fig. 6(b). However, in the current research work, since we are interested in the ultimate strength analysis under combined global and local loads, the numerical models are extended over two-hold $^1/_2 + 1 + {}^1/_2$. This is considered a reasonable model extension when analyzing the effect of lateral loads over the ultimate strength of container ships. It was previously shown by Fujikubo and Tatsumi [27],Matsumoto et al. [31],Tatsumi and Fujikubo [32] that a numerical model extended over two-hold captures the bottom bending effect accurately.

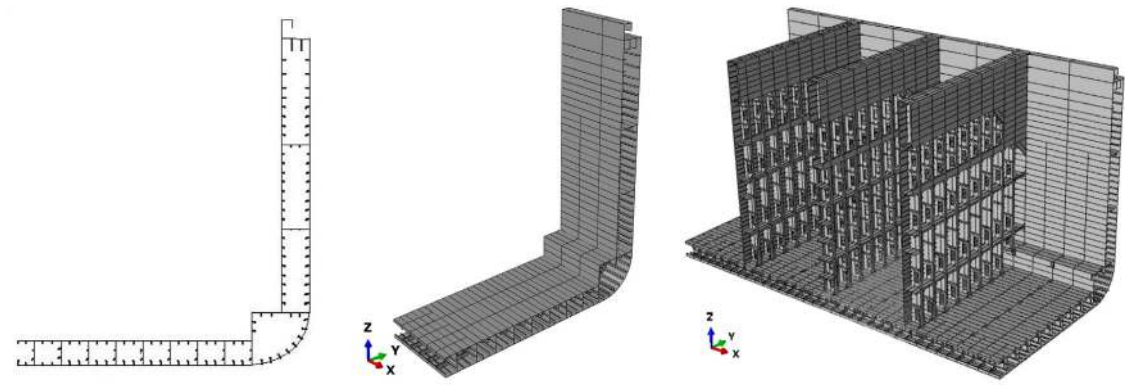

Fig. 6. 16,000 TEU container ship.

Fig. 7. Finite element model of 16,000 TEU container ship, extent of the collapse area.

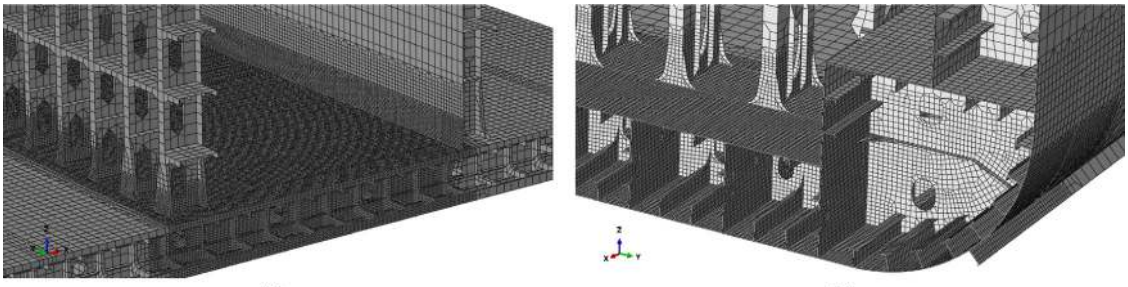

Fig. 8. Close-up view of the finite element mesh in the collapse area.

3.2. Finite element models and initial imperfections

For the model extended over 1/2 + 1 + 1/2-hold, the geometry of the ship is modeled with a high detail level, and the FE model is generated using the ABAQUS CAE interface. The element of choice in this work is S4: a general shell element with four nodes, which can be used for both thin and thick shells as well as small and large strain applications.

The area where collapse is expected to occur is modeled with higher density, as Fig. 7 bears out. The size of the elements in the collapse area is around 100 mm, usually eight elements over the spacing between stiffeners, as per best practice. The aspect ratio of each element is as close as possible to 1:1. It should be mentioned that the remaining part of the structure, far away from the collapse area, is modeled with shell elements of around 300 × 300 mm in size. The FE model of some structural details is depicted in Fig. 8. The finite element model contains more than two million degrees of freedom.

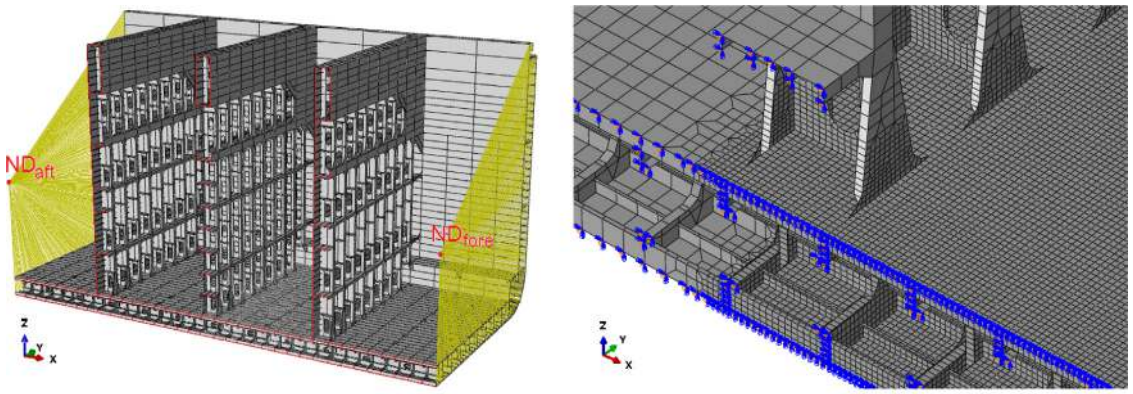

Fig. 9. Boundary conditions.

The initial imperfections are applied on the double bottom structure and are defined using analytical expressions to modify the position of the nodes, as proposed by Paik [56]. Three types of initial geometric imperfections are considered:

- local plate imperfections, defined as: $w_{pl} = A_{pl} \cdot \sin {}^{n_{hw}\pi x}/_{a} \cdot \sin {}^{\pi y}/_{b}$, where the maximum amplitude is a function only of the distance between stiffeners: $A_{pl} = 0.005 \cdot b$;
- global column type imperfections of plate between primary supporting members, defined as: $w_{col} = A_{col} \cdot \sin {}^{\pi x}/_{a} \cdot \sin {}^{\pi y}/_{b}$, where the maximum amplitude is a function only of the distance between girders: $A_{col} = 0.001 \cdot a$;
- global stiffeners torsional imperfections, defined as: $w_{tor} = A_{tor} \cdot {}^{z}/_{h_w} \cdot \sin {}^{\pi x}/_{a}$, where the maximum amplitude is a function only of the distance between girders: $A_{tor} = 0.001 \cdot a$.

where a is the stiffeners span, b is the stiffeners spacing, h_w is the stiffeners' web height. The number of half-waves in the longitudinal direction denoted as n_{hw}, for a plate subjected to axial compression is determined as the smallest integer value that satisfies Eq. (5), proposed by Paik [56].

$$\frac{a}{b} \leq \sqrt{(n_{hw}\,(n_{hw}+1))} \tag{5}$$

Additionally, it should be mentioned that for the FE model extended over three frame-bay, a similar mesh density and definition of initial imperfections are used. A detailed description of this model can be found in [39].

3.3. Material properties

The structural components are built from mild steel (σ_y=235MPa) and high tensile steels (σ_y=315, 355, 390, 460 MPa) with Young's modulus of 205.8 GPa and a Poisson ratio of 0.3. In the numerical analysis, the materials are defined with a bi-linear elastic–plastic model, including strain hardening with a slope of 1/1000. In order to analyze the strain rate effect on the hull girder's ultimate strength, the following constants [56]: C=3200, q=5 for high tensile steels and respectively C=40.4, q=5 for mild steel, are used for the Cowper–Symonds constitutive material model, presented in Eq. (2).

3.4. Boundary conditions

In the analysis of the hull girder ultimate strength, the following boundary conditions are adopted. The fore- and the aft-end cross-sections of the model are assumed to be rigid. A master node is set on the cross-sections, and the rest of the nodes are linked to the master node by rigid body elements. The model is simply supported at the master nodes, denoted by ND_{aft}, and ND_{fore}, respectively, as illustrated in Fig. 9(a). Since both the ship's structure and loadings are symmetrical with respect to the centerline, only half of the ship is modeled. Therefore the symmetrical condition is imposed on the centerline. Moreover, it is worth mentioning that the stiffeners located on the centerline are modeled with half thickness, and their lateral deflection is allowed. A detailed view of the boundary conditions on the centerline is shown in Fig. 9(b)

3.5. Loading conditions

This research's main objective is to investigate the influence of dynamic effects associated with slamming-induced whipping. Hence, two scenarios are considered: a *wave* scenario, and a *wave+whipping* scenario. In a *wave+whipping* scenario, the high-frequency whipping-induced stresses are superimposed to the low-frequency wave-induced stresses.

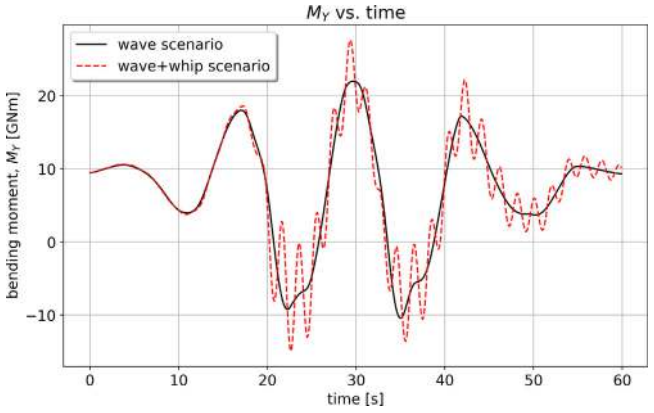

Fig. 10. Time histories of vertical bending moment for wave and wave+whipping scenario.

Table 2
Quasi-static ultimate strength.

Model	Loading condition	$M_{U\ quasi-static}$ [GNm]	
		w/o imp.	w/ imp.
Smith method	Pure bending	34.40	–
3FB FEM	Pure bending	34.78	31.48
2HM FEM	Pure bending	34.90	31.65
2HM FEM	Full load	32.31	29.05
2HM FEM	One-bay empty	30.72	27.37

In order to maintain a realistic ratio between the two load components and to have realistic periods, the load amplitude curves of the bending moments are obtained from a direct hydroelastic analysis. The hydroelastic analysis is performed by coupling a 3D-BEM model to solve the sea-keeping problem and the 1D-FEM model for the structural problem. The coupling is performed using the generalized modes approach, as presented in Section 2.3. The time histories are obtained using an equivalent design wave that maximizes the vertical bending moment at midship and are shown in Fig. 10. For both models, i.e., three frame-bay and two-hold, the bending moment is applied as concentrated loads on the two master nodes located at the aft- and fore-end of the model, using the same magnitude but opposite direction.

Furthermore, for the model extended over $1/2+1+1/2$-hold, the container loads are applied as concentrated masses on the double bottom and on the hatch coaming. The 40-foot container support plates are modeled as per the structural drawings. The design load for the container support structure in the cargo hold is 330 tones per 40-foot container stack, while for each stack on deck or hatch cover is 160 tones. Aside from that, the total lateral loads acting on the hull girder are composed of the hydrostatic pressure corresponding to the design draught of 14.5 m, and the hydrodynamic pressure. The hydrodynamic pressures for the considered EDW are calculated as specified in [40]. The hydrodynamic pressure is applied using the load-amplitude curve of the wave bending moment.

The above mentioned load components are combined into three loading conditions, as follows:

- **pure bending condition**: only the external bending moment is applied on the two master nodes;
- **full-load condition**: the external bending moment is combined with the lateral loads and with an uniform cargo weight distribution;
- **one-bay empty condition**: the external bending moment is combined with the lateral loads and with one-bay empty cargo weight distribution.

4. Results and discussion

4.1. Quasi-static ultimate strength

At first, the collapse under quasi-static conditions (i.e., disregarding the strain rate and inertia effects) is analyzed for all loading conditions. The internal bending moments versus end rotations relationships are shown in Fig. 11. The ultimate strength without initial imperfections is shown as a dotted line, while the ultimate strength with imperfections is shown as a solid line. Moreover, Table 2 summarizes the ultimate strength values for hogging condition. The ultimate strength under pure bending obtained on the two-hold model denoted as 2HM, is compared to the value obtained on the three frame-bay model, denoted 3FB, and with the result obtained using the simplified Smith approach, as discussed in [39].

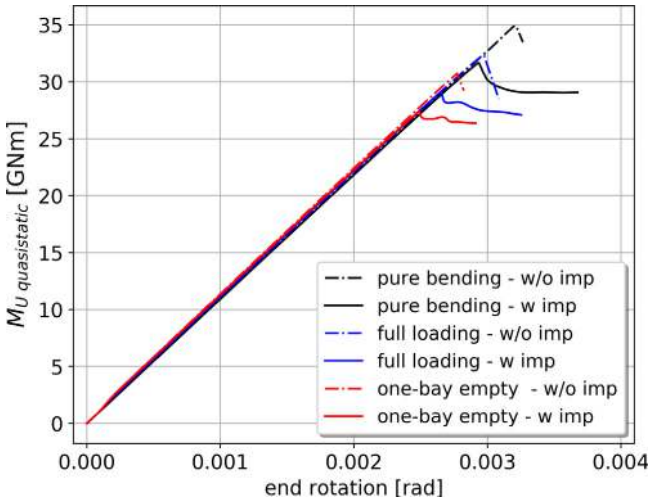

Fig. 11. Internal bending moment vs. end rotation relationships obtained on two-hold model.

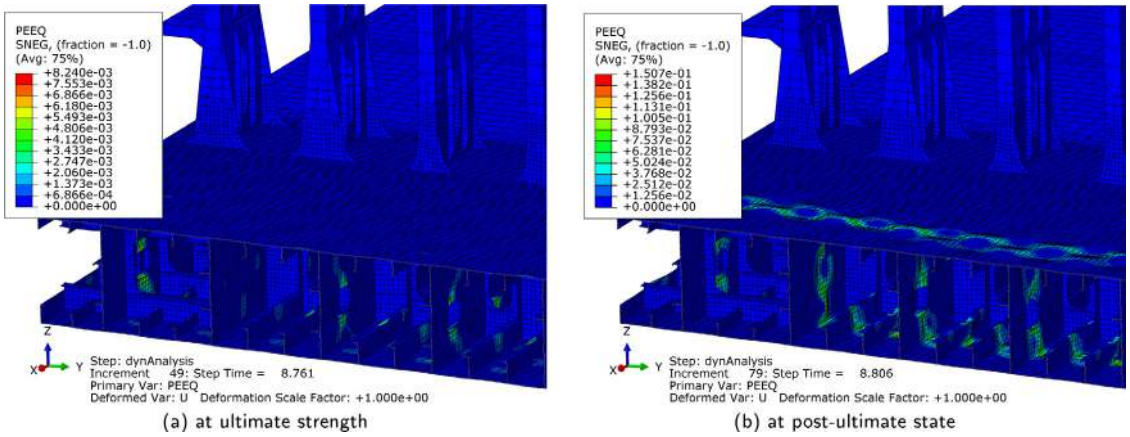

Fig. 12. Equivalent plastic strain distribution for the pure bending condition.

From Fig. 11 and Table 2, we can infer that there are two separate factors of ultimate strength reduction: initial imperfections and lateral loads effects. On the one hand, the initial imperfections are reducing the ultimate strength by about 10%. On the other hand, the lateral loads reduce the ultimate strength by 8.2% for the full-load condition and 13.5% for the one-bay empty condition compared to the quasi-static ultimate strength obtained two-hold model under pure bending condition. Moreover, it can be seen that the ultimate strength computed using the FE model extended over two-hold is in very good agreement with the value obtained using the model extended over three frame-bay.

Furthermore, the collapse behavior of the considered container ship is analyzed for all loading conditions. The distribution of equivalent plastic strain in the target bay at ultimate strength is depicted in Figs. 12(a), 13(a), and 14(a) for the pure bending, full loading, and one-bay empty conditions, respectively. In all cases, when the ultimate strength is reached, only the bottom plating and the attached stiffeners show concentrated plastic strains. Aside from that, it can be seen that on the side girders, some plastic strains are visible under the manholes.

Figs. 12(b), 13(b), and 14(b) show the distributions of equivalent plastic strain in the target bay in the post-collapse state. For the pure bending and one-bay empty conditions, the post-collapse behavior is similar: the buckling extends to the middle of the inner bottom plating. On the other hand, for the full loading condition, the buckling of the inner bottom plating appears next to the partial support bulkhead, where the 40-foot container support plates are located and where the vertical force of the cargo stacks is distributed.

Moreover, it should be noted that the deformation of the bottom stiffeners is different between the pure-bending scenario and lateral-load scenarios. A detailed view is presented in Fig. 15 where it can be seen that under bottom pressure, all the stiffeners are deflecting towards the side shell, while under pure bending, the deflection of stiffeners is symmetrical. This behavior is driven by the global deflection of the double bottom structure under local loads, which can be seen as a convex deflection in both transverse and longitudinal directions.

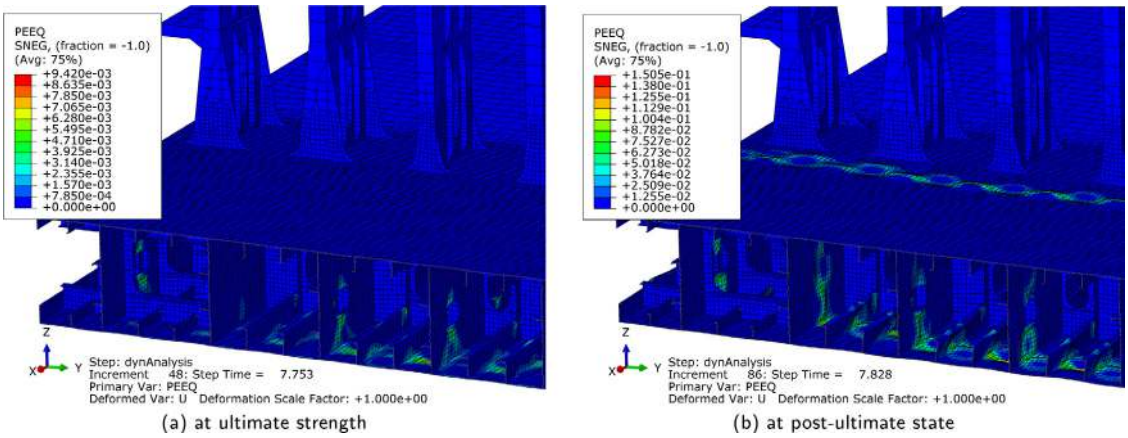

Fig. 13. Equivalent plastic strain distribution for the full load condition.

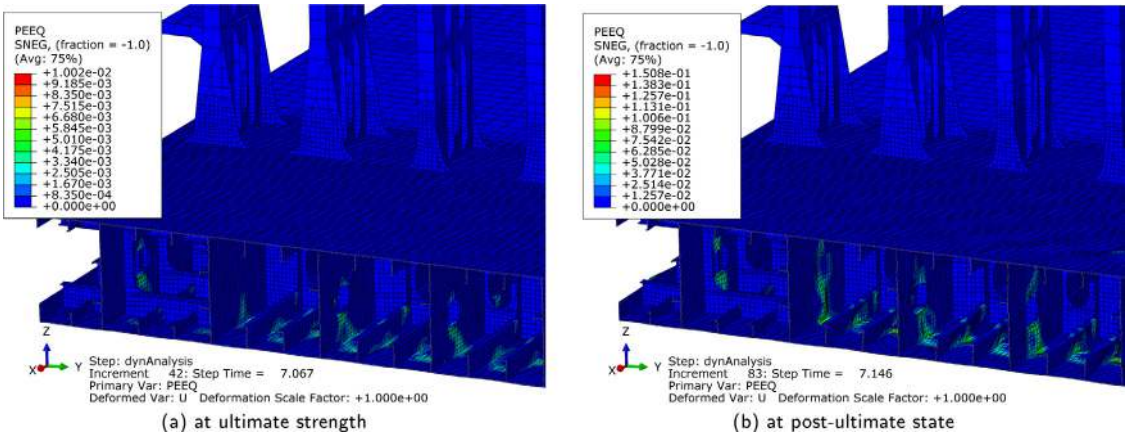

Fig. 14. Equivalent plastic strain distribution for the one-bay empty condition.

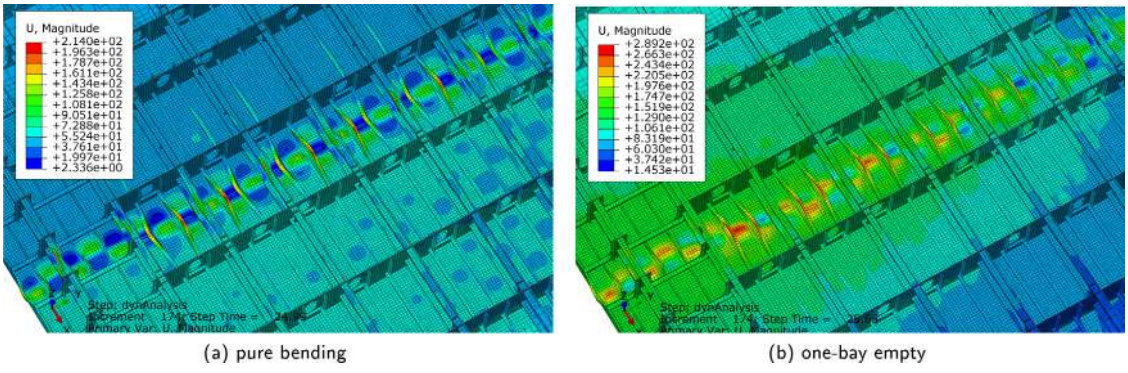

Fig. 15. Deflection of double bottom structure in post-ultimate state.

4.2. Dynamic ultimate strength

In order to quantify the influence of the dynamic effects over the structural capacity, the dynamic load factors are computed as the ratio between the dynamic ultimate strength and the quasi-static ultimate strength, as follows:

$$f_d = \frac{M_{U\ dynamic}}{M_{U\ quasi-static}} - 1 \tag{6}$$

Table 3
Dynamic load factors obtained for the three frame-bay model.

		$f_{d\ wave}$ [%]			$f_{d\ whip}$ [%]			γ_{DU} [%]
		T=12 s	T=10.5 s	T=8 s	T=2.1 s	T=1.8 s	T=1.6 s	
Half-sine	Jagite et al. [39]	5.8	6.0	6.1	7.9	8.0	8.2	
	Average value	5.96			8.03			1.95
EDW	Present work	T=11.8 s			T=1.85 s			
		5.5			6.9			1.32

The dynamic capacity, $M_{U\ dynamic}$, is obtained for the maximum load level that the structure can withstand; any higher load above this level will lead to structural failure. For practical reasons, the difference between a near-failure and a failure scenario is chosen as 0.001% of $M_{U\ quasi-static}$, as discussed in Section 2.1. Furthermore, as discussed in Section 2.2, the considered strain rate sensitivity model shows yield stress increased by around 5% at strain rates as low as 10^{-3} s^{-1}. However, this contradicts both the experimental results and the long-established industry practice. If one uses Eq. (6) to determine the dynamic load factor under wave-induced bending moment, it will find that the dynamic effects are about 5.5% (see Table 3). This capacity increase is an artifact of the considered strain rate model. In order to avoid this apparent increase, two possible methods can be adopted. The first method to obtain a correct interpretation of the influence of dynamic effects on the structural capacity is to determine the dynamic collapse effect as the ratio between the whipping and wave load scenarios, as shown in Eq. (7).

$$\gamma_{DU} = \frac{M_{U\ dynamic-whipping}}{M_{U\ dynamic-wave}} - 1 \tag{7}$$

The second method to avoid the inconsistencies of the Cowper–Symonds constitutive model is to use an improved strain rate sensitivity model. Such model, based on a piecewise definition has been proposed in [67]. For high-tensile steel, it follows:

$$\frac{\sigma_d}{\sigma_0} = \begin{cases} 1 & , \dot{\varepsilon} \le 10^{-3} \\ 1 + \dfrac{1}{a} \ln \dfrac{\dot{\varepsilon}}{10^{-3}} & , 10^{-3} < \dot{\varepsilon} \le \dot{\varepsilon}_0 \\ 1 + \left(\dfrac{\dot{\varepsilon}}{C}\right)^{1/q} & , \dot{\varepsilon_0} < \dot{\varepsilon} \end{cases} \tag{8}$$

with: $C = 3200$, $q = 5$, $a = 36.8$ and $\dot{\varepsilon}_0 = 0.148$.

The strain rate constitutive model presented in Eq. (8) shows no dynamic amplification for strain rates below 10^{-3} s^{-1}, while ensuring a smooth and continuous function for strain rates above 10^{-3} s^{-1}. At the same time, it maintains the accuracy of the original Cowper–Symonds model for strain rates above $\dot{\varepsilon}_0$. In [67] the dynamic ultimate strength of a stiffened panel has been analyzed for different wave-induced stress periods, ranging from 8 to 13 s. By using the new strain rate constitutive model, the dynamic load factor for wave loads is substantially smaller, from a $[4, 5]$% range to a $[0.5, 1.3]$% range, and it confirms the industry practice to consider the wave loads as "quasi-static". It is expected that the influence will be very close for the hull girder since similar strain rates are developed.

Both methods mentioned above yield very similar values for deriving the influence of dynamic effects over the structural capacity under slamming-induced whipping stresses. However, for simplicity, in the current research work, the first method has been adopted, computing the collapse effect as the ratio between the whipping and wave load scenarios, as shown in Eq. (7).

At first, the dynamic ultimate strength is calculated for the FE model extended over three frame-bay subjected to realistic pure bending loading scenario, noted as EDW, using a wave loading scenario, denoted as *wave*, and a wave+whipping loading scenario denoted as *whip*. The numerical results obtained on the three frame-bay model are summarized in Table 3, together with the results obtained under simplified half-sine loading scenarios extracted from [39]. Aside from that, it should be mentioned that for the considered EDW, the wave period is approximately 11.8 s, while the whipping period is about 1.85 s, as shown in Fig. 10.

From Table 3, we can infer that when the hull girder is subjected to a more realistic loading scenario, where the high-frequency whipping-induced stresses are superimposed to the low-frequency wave-induced ones, the dynamic effects will be smaller than the ones where simple half-sine loading scenarios are used. This aspect was also observed at the level of independent stiffened panels, as previously discussed in [67,68]. Thus, for the considered three frame-bay model, the average dynamic collapse effect obtained on simple half-sine loading scenarios is 1.95%, while under realistic EDW scenario, the dynamic collapse effect is reduced to 1.32%.

Furthermore, using the two-hold model, the dynamic ultimate strength is calculated for each loading condition using the *wave* loading and the *wave+whipping* loading scenarios. It is worth mentioning that within the iterative algorithm employed in the computation of the dynamic ultimate strength, the static components: still-water bending moment and hydrostatic pressures are kept constant. Moreover, the hydrodynamic pressures are kept constant, further study is necessary where the equivalent design wave height is increased. Thus, all the dynamic load components will be scaled at each iteration until the structure collapses. However, in the current research work, the dynamic ultimate strength is determined using the methodology described in Section 2.1 by scaling only the dynamic bending moment until the structure collapses. The numerical results obtained on the two-hold model are summarized in Table 4.

From the numerical results summarized in Table 4, it can be observed that the lateral loads are increasing the dynamic load factors. Moreover, it can be seen that the dynamic load factors obtained for the pure bending condition on the two-hold model

Table 4
Dynamic load factors obtained for the two-hold model under realistic loading scenarios (EDW).

Loading condition	$f_{d\ wave}$ [%]	$f_{d\ whip}$ [%]	γ_{DU} [%]
Pure bending	4.8	5.9	1.05
Full load	5.1	6.7	1.52
One-bay empty	6.0	8.4	2.26

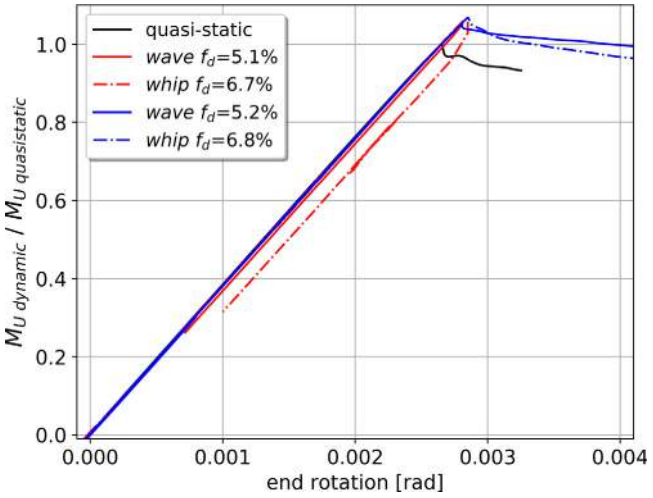

Fig. 16. Dynamic load factor vs. end rotation relationships for full load condition.

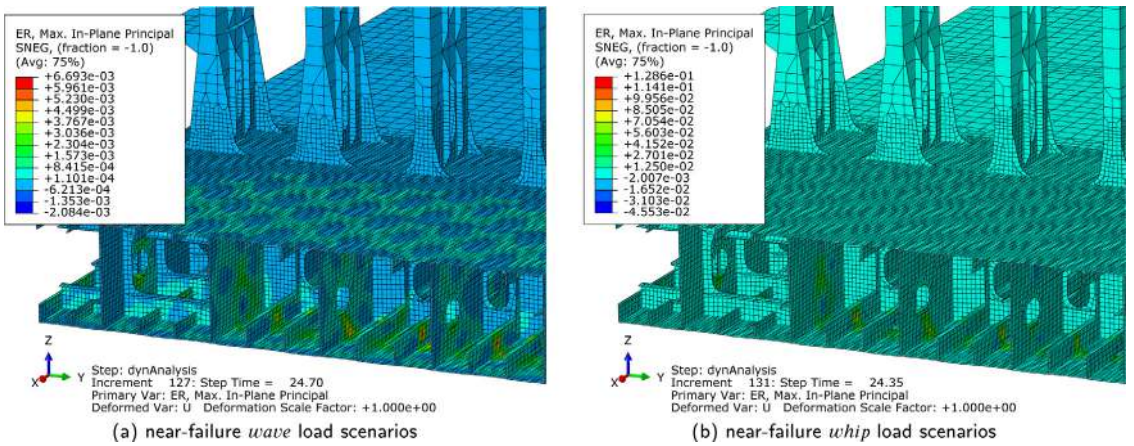

Fig. 17. Strain rate distribution for the pure bending condition.

($f_{d\ wave}$ = 4.8% and $f_{d\ whip}$ = 5.9%), are lower than the ones obtained on the three frame-bay model ($f_{d\ wave}$ = 5.5% and $f_{d\ whip}$ = 6.9%). To the authors' opinion, these differences are related to the model extension; a shorter model is stiffer due to the rigid elements used for the boundary conditions.

Furthermore, for the considered partial structural model extended over $^1/_2 + 1 + {}^1/_2$ holds, the dynamic collapse effect is about 1.05% when the structural model is subjected to a pure bending moment. On the other hand, for the full load condition, it is about 1.52%, and for the one-bay empty condition, it is about 2.26%. Hence, it can be concluded that the lateral loads are slightly increasing the dynamic capacity. This aspect was also observed in the analysis of local models such as one stiffened panels [67,68].

The collapse behavior and the localization of plastic strains for the dynamic ultimate strength analysis are similar to the ones from the quasi-static analysis; hence it will not be repeated hereafter. However, it should be mentioned that the strain rates obtained for the whipping loading scenario are usually with an order of magnitude higher than the ones obtained for the wave loading scenarios. The distributions of the strain rate for the near-failure *wave* and *whip* load scenarios are depicted in Figs. 17, 18, and 19, respectively.

If the load increases a little more, the structure fails, the aft- and fore-end rotations will accelerate rapidly. As a consequence, the local strain rates reached during collapse will be one or two orders of magnitude higher. Fig. 20 shows the strain rate distribution

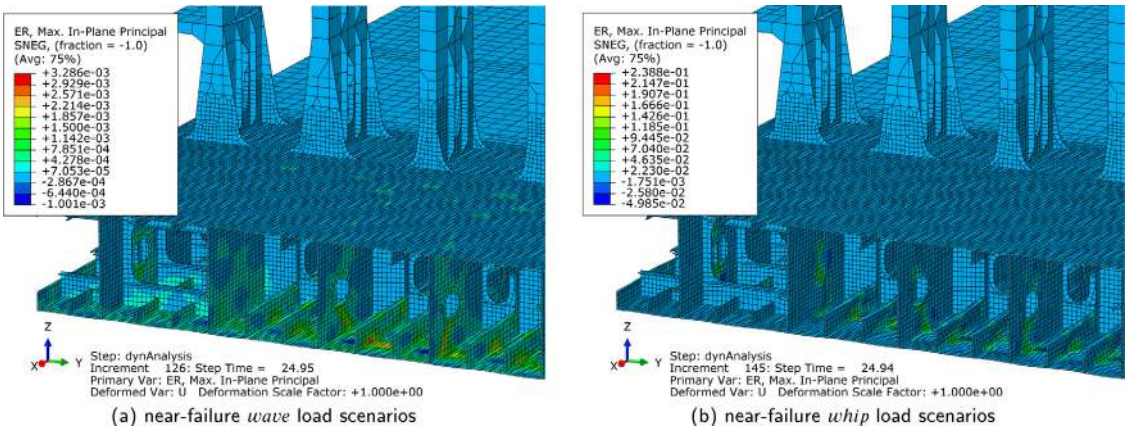

Fig. 18. Strain rate distribution for the full load condition.

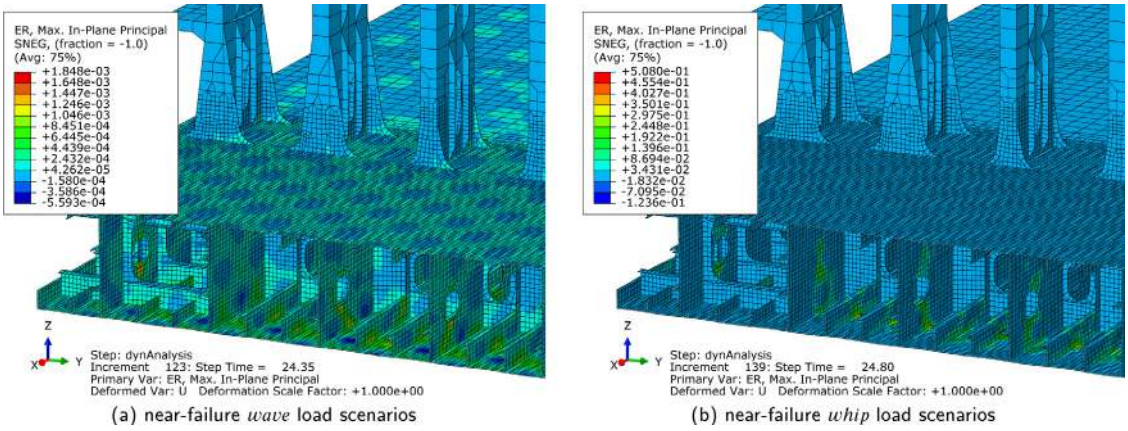

Fig. 19. Strain rate distribution for the one-bay empty condition.

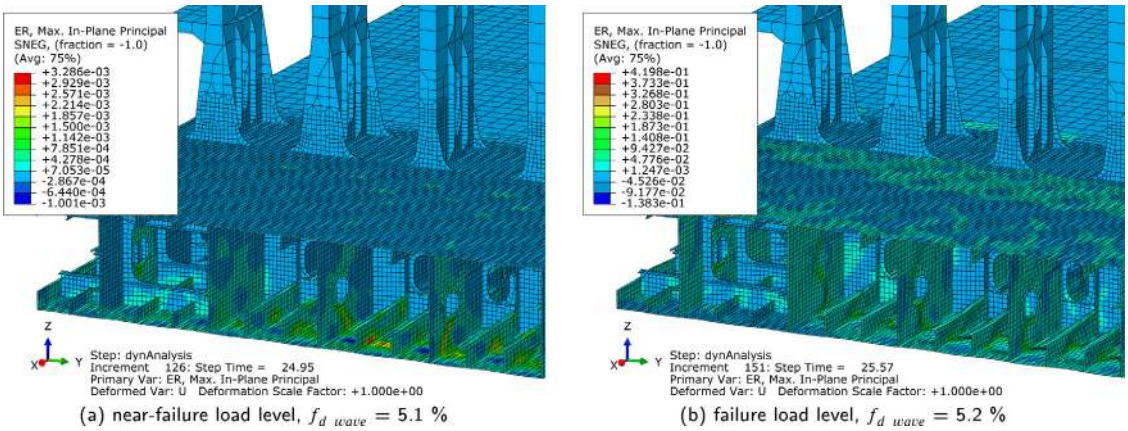

Fig. 20. Strain rate distribution for the *wave* load scenarios under full load condition.

for a *wave* load scenario under full load condition. The maximum strain rate obtained for a near-failure load level is about $3.2 \cdot 10^{-3}$ s^{-1}, while the maximum strain rate achieved during the collapse, for a slightly higher load-level, is about 0.42 s^{-1}.

Furthermore, as presented in Fig. 10, the time series of the external bending moment contains several loading cycles. It is important to mention that after the first hogging loading cycle is completed, the structure shows only some plastic strains located

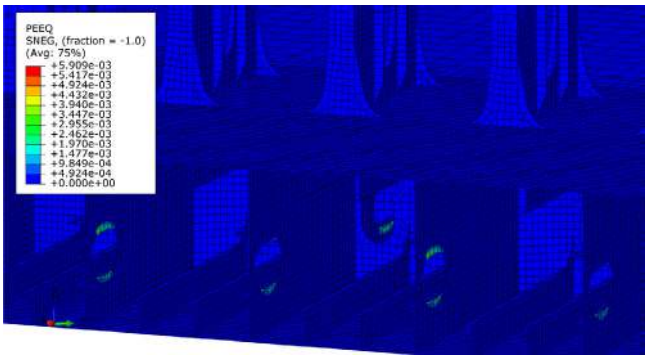

Fig. 21. Equivalent plastic strain distribution after the first hogging loading cycle.

on the side girders within the double bottom structure, as depicted in Fig. 21. These limited plastic deformations do not affect the unloading and/or the loading path for the following hogging loading cycle, as shown in Fig. 16.

5. Conclusions

This paper presents a series of dynamic collapse analyses for a 16 000 TEU container ship. Two finite element models with different longitudinal extensions are used: a three frame-bay model and a two-hold model. The partial structural models are subjected to various loading scenarios representative of the wave-induced stresses and whipping-induced stresses. Moreover, to analyze the effect of combined bending moment and lateral loads over the dynamic ultimate strength, the two-hold model is subjected to three different loading conditions: pure bending, full load, and one-bay empty. The load amplitude curves of the vertical bending moment for the *wave* scenario and *wave+whipping* scenario are computed by direct hydroelastic analysis by subjecting the hull girder to an equivalent design wave.

At first, the quasi-static ultimate strength, i.e., without any dynamic effects, is calculated using the arc-length method and the simplified Smith method. The numerical results obtained for the pure bending condition on the three frame-bay model are in very good agreement with those on the two-hold model and the ones obtained using the simplified Smith method. Moreover, it is confirmed that two major factors are reducing the hull girder capacity, named: *initial imperfections*, with a reduction of about 10%, and *lateral loads*, with an additional reduction between 8.2% and 13.5%.

Furthermore, the dynamic ultimate strength is calculated using the implicit NL-FEM solver existent in [69], where both material and geometrical nonlinearities are taken into account. It should be mentioned that the strain rate sensitivity effect is described using the well-known Cowper–Symonds model. The dynamic capacity is determined using an iterative approach, where each iteration requires an independent time-domain analysis to be performed. More importantly, the dynamic capacity is defined as the maximum load that the structure can withstand without collapsing, any higher load level would lead to a structural failure. In order to quantify the influence of the dynamic effects, the dynamic load factors are computed as the ratio between the dynamic ultimate strength and the quasi-static one. The dynamic load factors vary between 4.8% and 6.0% for a $wave$ loading scenario and between 5.9% and 8.4% for a $whipping$ loading scenario.

However, the long-established industry practice considers the wave loads as quasi-static and disregards any dynamic effects associated with the wave loads. Thus, it is decided to compute the dynamic collapse effect as the relative value between $whipping$ and $wave$ scenarios. Therefore, the dynamic collapse effect can be used to quantify the increase of structural capacity due to slamming-induced whipping. For the considered ship, the dynamic collapse effect varies from 1.05% to 2.26%. The lowest value is obtained for the pure-bending loading condition, while the highest value is for the one-bay empty condition. It can be concluded that the lateral loads are leading to a higher dynamic collapse effect. Similar behavior was observed on the analysis of stiffened panels under in-plane compression and lateral loads, presented in [68].

Finally, this paper completes a series of investigations reported by the authors on the dynamic ultimate strength analysis. The main objective was to determine how the dynamic effects associated with the slamming-induced whipping are affecting the structural capacity. For the considered 16 000 TEU container ship, the dynamic collapse effect obtained for simple half-sine pure bending moments on a three-frame bay model varies from 1.8% to 2.2%. Moreover, when using an extended two-hold model under realistic loading scenarios, the dynamic collapse effect varies from 1.05% to 2.26%. Therefore, it seems that the usual assumption that the strain rate effect is negligible in the analysis of the ultimate strength of ship structures subjected to wave load can be extended to the analysis of structures subjected to whipping-induced stresses.

Declaration of competing interest

The authors declare that they have no known competing financial interests or personal relationships that could have appeared to influence the work reported in this paper.

Acknowledgments

The present research work was undertaken at Ecole Centrale de Nantes, France, as a part of a Ph.D. thesis on the analysis of whipping effects over the hull girder's ultimate strength. The first author is pleased to acknowledge the funding and support of Bureau Veritas via BV-ECN cooperation.

References

[1] Caldwell J. Ultimate longitudinal strength. Trans RINA 1965;107:411–30.
[2] Paik JK, Mansour AE. A simple formulation for predicting the ultimate strength of ships. J Mar Sci Technol 1995;1:52–62. http://dx.doi.org/10.1007/BF01240013.
[3] Paik J, Kim D, Park D, Kim H, Mansour A, Caldwell J. Modified paik-mansour formula for ultimate strength calculations of ship hulls. Ships Offshore Struct 2013;8:245–60. http://dx.doi.org/10.1080/17445302.2012.676247.
[4] Smith CS. Influence of local compressive failure on ultimate longitudinal strength of a ship's hull. In: Proc. int. sym. on practical design in shipbuilding, vol. 7. 1977, p. 3–79.
[5] Adamchak JC. ULSTR: a program for estimating the collapse moment of a ship's hull under longitudinal bending. In: David W, editor. Taylor Naval Ship Research and Development Center Bethesda MD. Technical Report, 1982.
[6] Yao T, Nikolov PI. Progressive collapse analysis of a ship's hull under longitudinal bending (2nd report). J Soc Naval Arch Jpn 1992;1992:437–46.
[7] S11A, IU. Longitudinal strength standard for container ships. 2015.
[8] Tanaka Y, Ogawa H, Tatsumi A, Fujikubo M. Analysis method of ultimate hull girder strength under combined loads. Ships Offshore Struct 2015;10:587–98.
[9] Fujikubo M, Tatsumi A. Progressive collapse analysis of a container ship under combined longitudinal bending moment and bottom local loads. In: Progress in the analysis and design of marine structures. CRC Press; 2017, p. 235–42.
[10] Ueda Y, Sherif R. An ultimate transverse strength analysis of ship structure. J Soc Naval Arch Jpn 1974;1974:309–24.
[11] Ueda Y, Rashed S. The idealized structural unit method and its application to deep girder structures. Comput Struct 1984;18.
[12] Ueda Y. Official discussion to the report of special task committee vi.2: Ultimate hull girder strength. In: Proc. 14th ISSC, Nagasaki, Japan, vol. 2. 2000, p. 319–27.
[13] Paik JK, Thayamballi AK, Che J, Pedersen P, Mansour A. Ultimate strength of ship hulls under combined vertical bending, horizontal bending, and shearing forces. discussion. authors' closure. Trans-Soc Naval Arch Mar Eng 1996;104:31–59.
[14] Paik J, Thayamballi A. A concise introduction to the idealized structural unit method for nonlinear analysis of large plated structures and its application. Thin-Walled Struct 2003;41:329–55.
[15] Fujikubo M, Yanagihara D, Setoyama Y, Olaru DV, et al. Isum approach for collapse analysis of double-bottom structures in ships. Int. J. Offshore Polar Eng. 2003;13.
[16] Underwood JM, Sobey AJ, Blake JI, Shenoi RA. Ultimate collapse strength assessment of damaged steel-plated structures. Eng Struct 2012;38:1–10.
[17] Lindemann T. Idealized structural unit method for collapse analyses of plate structures under inplane and lateral loads. (Ph.D. thesis), Universität Rostock; 2015.
[18] Kaeding P, Fujikubo M, et al. New simplified model for collapse analysis of stiffened plates and its application to offshore structures. Int J Offshore Polar Eng 2002;12.
[19] Paik JK, Kim BJ, Seo JK. Methods for ultimate limit state assessment of ships and ship-shaped offshore structures: Part iii hull girders. Ocean Eng 2008;35:281–6.
[20] Lindemann T, Kaeding P. Application of the idealized structural unit method for ultimate strength analyses of stiffened plate structures. Ship Technol Res 2017;64:15–29.
[21] Amlashi HK, Moan T. Ultimate strength analysis of a bulk carrier hull girder under alternate hold loading condition–a case study: Part 1: Nonlinear finite element modelling and ultimate hull girder capacity. Mar Struct 2008;21:327–52.
[22] Shu Z, Moan T. Ultimate strength of a capesize bulk carrier in hogging and alternate hold loading condition. In: ASME 2010 29th International conference on ocean, offshore and arctic engineering. American Society of Mechanical Engineers Digital Collection; 2010, p. 441–9.
[23] Pei Z, Yao T, Iijima K, Fujikubo M, Tanaka Y, Tanaka S, et al. Collapse behaviour of ship hull girder of bulk carrier under alternative heavy loading condition. In: The twenty-second international offshore and polar engineering conference. International Society of Offshore and Polar Engineers; 2012.
[24] IACS, C. Common structural rules for bulk carriers and oil tankers. 2014.
[25] Darie I, Roerup J, Wolf V. Ultimate strength of a cape size bulk carrier under combined global and local loads. In: Proc 12th symp practical design of ships and other floating structures. 2013, p. 1173–80.
[26] Pei Z, Iijima K, Fujikubo M, Tanaka S, Okazawa S, Yao T. Simulation on progressive collapse behaviour of whole ship model under extreme waves using idealized structural unit method. Mar Struct 2015;40:104–33.
[27] Fujikubo M, Tatsumi A. Ultimate strength of ship hull girder under combined longitudinal bending and local loads. In: Proc. of 2nd int. conf. on safety & reliability of ships, offshore & subsea structures (SAROSS2016). Glasgow; 2016.
[28] Tatsumi A, Fujikubo M. Finite element analysis of longitudinal bending collapse of container ship considering bottom local loads. In: ASME 2016 35th International conference on ocean, offshore and arctic engineering. American Society of Mechanical Engineers Digital Collection; 2016.
[29] Mohammed EA, Benson S, Hirdaris S, Dow R. Design safety margin of a 10, 000 teu container ship through ultimate hull girder load combination analysis. Mar Struct 2016;46:78–101.
[30] Tanaka Y, Hashizume Y, Ogawa H, Tatsumi A, Fujikubo M. Analysis method of ultimate strength of ship hull girder under combined loads: Application to an existing container ship. In: ASME 2016 35th International conference on ocean, offshore and arctic engineering. American Society of Mechanical Engineers Digital Collection; 2016.
[31] Matsumoto T, Shigemi T, Kidogawa M, Ishibashi K, Sugimoto K. Examination of effect of lateral loads on the hull girder ultimate strength of large container ships. In: ASME 2016 35th International conference on ocean, offshore and arctic engineering. American Society of Mechanical Engineers; 2016.
[32] Tatsumi A, Fujikubo M. Ultimate strength of container ships subjected to combined hogging moment and bottom local loads part 1: Nonlinear finite element analysis. Mar Struct 2020;69:102683.
[33] Iijima K, Kimura K, Xu W, Fujikubo M. Hydroelasto-plasticity approach to predicting the post-ultimate strength behavior of a ship's hull girder in waves. J Mar Sci Technol 2011;16:379–89.
[34] Xu W, Iijima K, Fujikubo M. Investigation into post-ultimate strength behavior of ship's hull girder in waves by analytical solution. In: ASME 2011 30th International conference on ocean, offshore and arctic engineering. American Society of Mechanical Engineers Digital Collection.; 2011, p. 455–62.
[35] Derbanne Q, de Lauzon J, Bigot F, Malenica S. Investigations of the dynamic ultimate strength of a ship's hull girder during whipping. Proc. PRADS 2016;2016(4).
[36] Iijima K, Fujikubo M. Hydro-elastoplastic behaviour of vlfs under extreme vertical bending moment by segmented beam approach. Mar Struct 2018;57:1–17.
[37] DNVGL CG-0153. Fatigue and ultimate strength assessment of container ships including whipping and springing. Det Norske Veritas; 2015.

[38] Yamada Y. Dynamic collapse mechanism of global hull girder of container ships subjected to hogging moment. J Offshore Mech Arct Eng 2019;141:051605.
[39] Jagite G, Le Sourne H, Cartraud P, Bigot F, Derbanne Q, Malenica Š. Examination of the dynamic effects on the hull girder ultimate strength of ultra large container ships. In: Trends in the analysis and design of marine structures: proceedings of the 7th international conference on marine structures. CRC Press; 2019b, p. 137–49.
[40] BV NR 625. Structural Rules for Container Ships. Bureau Veritas; 2019.
[41] S34, IU. Functional requirements on load cases for strength assessment of container ships by finite element analysis. 2015.
[42] Jiang L, Zhang S, White N. Nonlinear finite element dynamic collapse analyses of stiffened panels. In: Proceedings of the sixth international conference on hydroelasticity in marine technology. Tokyo, Japan; 2012, p. 19–21.
[43] Manjoine M. Influence of rate of strain and temperature on yield stresses of mild steel. J Appl Mech-Trans ASME 1945;12:A186.
[44] Cowper GR, Symonds PS. Strain-hardening and strain-rate effects in the impact loading of cantilever Beams. Technical report, Brown Univ Providence Ri; 1957.
[45] Campbell J, Cooper R. Yield and flow of low-carbon steel at medium strain rates. Inst Phys Phys Soc 1966;7:7–87.
[46] Rolfe ST, Rhea DM, Kuzmanovic BO. Ship structures committee. Report, 1974, volume 244.
[47] Francis P, Cook T, Nagy A. Ship structures committee. report. SSC-275, 1978a.
[48] Francis PH, Cook T, Nagy A. The effect of strain rate on the toughness of ship steels. Technical report, Southwest Research Institute; 1978b.
[49] Jones N. Structural impact. Cambridge University Press; 2011.
[50] Choung J, Nam W, Lee JY. Dynamic hardening behaviors of various marine structural steels considering dependencies on strain rate and temperature. Mar Struct 2013;32:49–67.
[51] Paik JK, Kim KJ, Lee JH, Jung BG, Kim SJ. Test database of the mechanical properties of mild, high-tensile and stainless steel and aluminium alloy associated with cold temperatures and strain rates. Ships Offshore Struct 2017;12:S230–56.
[52] Lee H, Kim B. A study on the application of material properties in ship collision analysis. In: Proceedings of the annual autumn meeting SNAK. 2007, p. 1050–7.
[53] BV NR 216. Rules on Materials and Welding for the Classification of Marine Units. Bureau Veritas; 2018.
[54] DNVGL, OS-B101. Metallic-materials. Det Norske Veritas; 2021.
[55] ISO E. 6892-1. Metallic materials-tensile testing-part 1: Method of test at room temperature. International Organization for Standardization; 2009.
[56] Paik JK. Ultimate limit state design of steel-plated structures. 2nd ed.. John Wiley & Sons; 2018.
[57] Tuitman J, Malenica Š. Fully coupled seakeeping, slamming, and whipping calculations. In: Proceedings of the institution of mechanical engineers, part m: Journal of engineering for the maritime environment, vol. 223. 2009, p. 439–56.
[58] Cummins W. The impulse response function and ship motions. Technical report, David Taylor Model Basin Washington DC; 1962.
[59] De Lauzon J, Grgic M, Derbanne Q, Malenica S. Improved generalized wagner model for slamming. In: Proceedings of 7th international conference on hydroelasticity in marine technology. Split, Croatia; 2015, p. 561–74.
[60] Derbanne Q, Malenica J, Bigot F, Chen X. Validation of the global hydroelastic model for springing & whipping of ships. In: 11th International symposium on practical design of ships and other floating structures. Rio de Janeiro; 2010, p. 331–40.
[61] BV NI 638. Guidance for Long-Term Hydro-Structure Calculations. Bureau Veritas; 2019.
[62] Hogben N (Neil), Dacunha NMC, Olliver GF, Ltd BMT. Global wave statistics. London; 1986, c1986. A forerunner of this book enitled 'Ocean Wave statistics' was published 1967.
[63] Dietz JS. Application of conditional waves as critical wave episodes for extreme loads on marine structures. (Ph.D. thesis), Technical University of Denmark (DTU; 2005.
[64] De Hauteclocque G, Derbanne Q, El-Gharbaoui A. Comparison of different equivalent design waves with spectral analysis. In: ASME 2012 31st International conference on ocean, offshore and arctic engineering, american society of mechanical engineers. 2012, p. 353–61.
[65] de Hauteclocque G, Derbanne Q, Mienahou T. Non linearity of extreme vertical bending moment: Comparison of design wave approaches and short term approaches. In: ASME 2013 32nd International conference on ocean, offshore and arctic engineering. American Society of Mechanical Engineers; 2013.
[66] Jagite G, Derbanne Q, Malenica S, Bigot F, Le Sourne P. Investigation of the nonlinear slamming-induced whipping response of ships using a fully-coupled hydroelastoplastic method. Ocean Eng 2021;238:109751. http://dx.doi.org/10.1016/j.oceaneng.2021.109751, https://www.sciencedirect.com/science/article/pii/S0029801821011185.
[67] Jagite G, Bigot F, Derbanne Q, Malenica Š, Le Sourne H, de Lauzon J, et al. A parametric study on the dynamic ultimate strength of a stiffened panel subjected to wave- and whipping-induced stresses. Ships Offshore Struct 2020;1–15. http://dx.doi.org/10.1080/17445302.2020.1790985.
[68] Jagite G, Bigot F, Derbanne Q, Malenica Š, Le Sourne H, de Lauzon J, et al. Numerical investigation on dynamic ultimate strength of stiffened panels considering real loading scenarios. Ships Offshore Struct 2019a;1–13. http://dx.doi.org/10.1080/17445302.2019.1601329.
[69] ABAQUS. Dassault Systemes Simulia Corp. RI USA: Johnston; 2017.